

The sliding phase transition in ferroelectric van der Waals bilayers

Ping Tang¹ and Gerrit E. W. Bauer^{1,2,3,4,5}

¹WPI-AIMR, Tohoku University, 2-1-1 Katahira, Sendai 980-8577, Japan

²Institute for Materials Research, Tohoku University, 2-1-1 Katahira, Sendai 980-8577, Japan

³Center for Spintronics Research Network, Tohoku University, Sendai 980-8577, Japan

⁴Zernike Institute for Advanced Materials, University of Groningen, 9747 AG Groningen, Netherlands and

⁵Kawli Institute for Theoretical Sciences, University of the Chinese Academy of Sciences, Beijing 10090, China

We address the sliding thermodynamics of van der Waals-bonded bilayers by the continuum elasticity theory. We attribute the robustness of the ferroelectricity recently observed in h-BN and WTe₂ bilayers to large monolayer in-plane stiffness. We compute the electric susceptibility and specific heat in the mean-field self-consistent phonon approximation. We compare critical temperatures and electric switching fields with the observations.

The discovery of ferroelectricity in van der Waals stacked bilayers of two-dimensional (2D) WTe₂ and hexagonal boron nitride (h-BN) with out-of-plane polarization substantially expands the family of ferroelectric materials [1–9]. The dipolar order arises from the precise stacking of two polar van der Waals-bonded monolayers that change sign by a small shear motion. The potential barriers for switching between the up and down polarization states are very low (\lesssim meV per unit cell) [1, 2, 8]. Surprisingly, the “sliding ferroelectricity” remains stable even above room temperature [4, 6, 7, 9], in contrast to the ferromagnetism in van der Waals mono or bilayers [10–17].

From a theoretical perspective, long-range order weakens with reduced dimensionality (d) [18]. According to the Mermin-Wagner-Hohenberg theorem [19, 20] at any finite temperatures an isotropic short-range force cannot order spin system with $d \leq 2$ due to the infrared divergence caused by gapless Goldstone modes. An anisotropy or a switching barrier is thus essential for phase transitions in $d \leq 2$. 2D magnets are stable at room temperature only when the magnetic anisotropy amounts to tens of meV per magnetic moment. The mechanism underlying the high thermal stability of sliding ferroelectrics in spite of the low switching barriers appears to be unexplained.

In this Letter we present a thermodynamic model of 2D sliding ferroelectrics that explains this conundrum. We associate the sliding ferroelectric phase transition with the shear motion of the entire layer with macroscopic mass that is driven by thermally fluctuating forces. The model parameters include the mass density, intralayer stiffness, and interlayer bonding. The phase transition is triggered by a soft “sliding phonon” of the bilayers and the high Curie temperature follows from the interplay between the ultralow switching barrier and intralayer rigidity. This mechanism is not unique for ferroelectrics, but also holds for structural sliding instabilities in non-ferroelectric bilayers, in which the phase transition can be observed in the specific heat. However, the ferroelectricity serves as a unique monitor of a bistability that can be controlled by temperature-dependent critical switch-

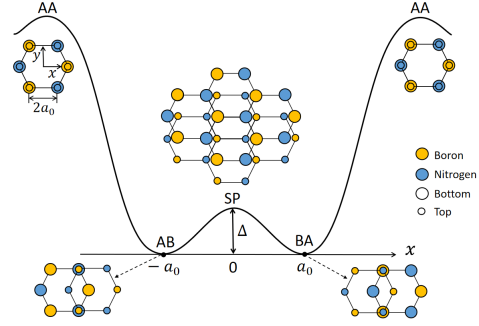


FIG. 1. The interlayer binding energy landscape in sliding ferroelectrics illustrated for hexagonal BN bilayers. The AB and BA stacking configurations correspond to two opposite spontaneous polarization states that are separated by saddle-shaped potential with minimum energy barrier Δ (per unit area). Boron and nitrogen atoms in the top (bottom) layer are represented by large (small) orange and blue circles, respectively.

ing fields.

We consider a bilayer of two atomic monolayers that may slide relative to each other along a particular direction, e.g., the armchair (long lattice vector) direction in the parallel stacked h-BN (WTe₂) bilayer. The energy minima correspond to states with opposite polarity that are separated by a saddle-point (SP) potential barrier (Δ) defined by an intermediate non-polar configuration, as sketched in figure 1. In the presence of a perpendicular electric field E , the Hamiltonian of a bilayer under a relative sliding displacement \hat{u}_s along the x direction reads [21, 22]

$$\hat{H} = \int \left[\frac{\hat{\pi}_s^2}{2\rho_s} + \frac{\lambda + 2\mu}{2} \left(\frac{\partial \hat{u}_s}{\partial x} \right)^2 + \frac{\mu}{2} \left(\frac{\partial \hat{u}_s}{\partial y} \right)^2 \right] d^2\mathbf{r} + \int [V_B(\hat{u}_s) - EP(\hat{u}_s)] d^2\mathbf{r}, \quad (1)$$

where $\rho_s = \rho/2$ is half of the mass density ρ of a single layer, $\hat{\pi}_s = \rho_s \dot{\hat{u}}_s$ the conjugate momentum to \hat{u}_s , λ and μ the 2D Lamé coefficients, and V_B the interlayer

binding energy density. $P(\hat{u}_s)$ is the electric polarization density that depends on \hat{u}_s and should be evaluated self-consistently below. Here we consider only one-component sliding motion, disregarding the interlayer displacements that do not directly affect the polar states such as out-of-plane flexural modes. We also neglect weak modulations of the electrostatic energy beyond the Stark interaction $-EP$.

$P(\hat{u}_s)$ is an odd function of \hat{u}_s with respect to the non-polar SP, to leading order therefore $P(\hat{u}_s) = Z\hat{u} + \mathcal{O}(\hat{u}_s^3)$, where Z is a constant that measures the interlayer polarization by the ionic charges. When $Z = 0$, the electric polarization and field effect vanish; our model then describes a sliding structural phase transition between degenerate ground states [23].

$V_B(\hat{u}_s)$ is in general periodic for a large sliding distance. However, since the polar states are usually separated by a very low barrier and a small sliding displacement, we may adopt an approximate inverted camel-back potential [2]

$$V_B(\hat{u}_s) = \frac{\Delta}{a_0^4} (\hat{u}_s^2 - a_0^2)^2 \quad (2)$$

where Δ represents the barrier height per unit area and $2a_0$ is the distance between the two minima. When $E = 0$, Eq. (2) hosts two degenerate minima at $\pm a_0$ with polarization $P_0 = \pm Z a_0$.

In general

$$\hat{u}_s(\mathbf{r}, t) = \langle \hat{u}_s \rangle + \hat{\xi}_s(\mathbf{r}, t) \quad (3)$$

where $\langle \dots \rangle$ denotes the thermal average, $\hat{\xi}_s(\mathbf{r}, t)$ are the spatio-temporal fluctuations with $\langle \hat{\xi}_s(\mathbf{r}, t) \rangle = 0$, and $\langle \hat{\xi}_s^n(\mathbf{r}, t) \rangle = \langle \hat{\xi}_s^n \rangle$ is independent of time and space. At equilibrium the force on each layer vanishes, i.e.,

$$\langle \hat{\pi}_s(\mathbf{r}, t) \rangle = -\frac{i}{\hbar} \langle [\hat{\pi}_s(\mathbf{r}, t), \hat{\mathcal{H}}] \rangle = 0. \quad (4)$$

With Bosonic commutation relations $[\hat{\pi}_s(\mathbf{r}, t), \hat{u}_s(\mathbf{r}', t)] = -i\hbar\delta(\mathbf{r} - \mathbf{r}')$ and $[\hat{\pi}_s(\mathbf{r}, t), \hat{\pi}_s(\mathbf{r}', t)] = 0$, Eq. (4) leads to

$$\langle \hat{u}_s \rangle^3 + 3\langle \hat{u}_s \rangle \langle \hat{\xi}_s^2 \rangle + \langle \hat{\xi}_s^3 \rangle - a_0^2 \langle \hat{u}_s \rangle = \frac{Z a_0^4 E}{4\Delta} \quad (5)$$

since the spatial gradient terms in Eq. (1) vanish on average. The dynamic equation for the fluctuations can be found from Heisenberg's equation of motion, $\hat{\pi}_s = (-i/\hbar)[\hat{\pi}_s, \hat{\mathcal{H}}]$, as

$$\begin{aligned} \rho_s \ddot{\xi}_s &= \frac{\lambda + 2\mu}{2} \frac{\partial^2 \hat{\xi}_s}{\partial x^2} + \frac{\mu}{2} \frac{\partial^2 \hat{\xi}_s}{\partial y^2} \\ &- \frac{4\Delta}{a_0^4} \left[\left(\langle \hat{u}_s \rangle + \hat{\xi}_s \right)^3 - a_0^2 \left(\langle \hat{u}_s \rangle + \hat{\xi}_s \right) \right] + ZE. \end{aligned} \quad (6)$$

We solve Eqs. (5) and (6) in the self-consistent phonon scheme [24, 25] using the mean-field approximations $\hat{\xi}_s^2 \approx$

$\langle \hat{\xi}_s^2 \rangle$ and $\hat{\xi}_s^3 \approx 3\langle \hat{\xi}_s^2 \rangle \hat{\xi}_s$. Eq. (5) then reduces to

$$\langle \hat{u}_s \rangle \left(\langle \hat{u}_s \rangle^2 + 3\langle \hat{\xi}_s^2 \rangle - a_0^2 \right) = \frac{Z a_0^4 E}{4\Delta}. \quad (7)$$

When $E = 0$, two roots are ferroelectric $\langle \hat{u}_s \rangle = \pm(a_0^2 - 3\langle \hat{\xi}_s^2 \rangle)^{1/2}$ and one is paraelectric $\langle \hat{u}_s \rangle \equiv 0$. With Eq. (7), we can rewrite Eq. (6) in the form of a harmonic oscillator in momentum space with $\xi_s(\mathbf{q}, t) = \int d^2\mathbf{r} \xi_s(\mathbf{r}, t) e^{-i\mathbf{q}\cdot\mathbf{r}}$

$$\ddot{\xi}_s(\mathbf{q}, t) = -\Omega_{\mathbf{q}}^2 \hat{\xi}_s(\mathbf{q}, t), \quad (8)$$

with frequency dispersion that acquires a gap $\sim \sqrt{\Delta}$:

$$\begin{aligned} \Omega_{\mathbf{q}} &= \frac{1}{\sqrt{\rho}} \left[\frac{8\Delta}{a_0^4} \left(3\langle \hat{u}_s \rangle^2 + 3\langle \hat{\xi}_s^2 \rangle - a_0^2 \right) + (\lambda + 2\mu)q_x^2 \right. \\ &\quad \left. + \mu q_y^2 \right]^{1/2}. \end{aligned} \quad (9)$$

Quantum mechanics enters the problem at low temperatures T and high frequencies when $\hbar\Omega_{\mathbf{q}} \gtrsim k_B T$, where \hbar (k_B) is Planck's (Boltzmann's) constant. The mean-square of the fluctuations from the equilibrium position of an ensemble of harmonic oscillators reads

$$\langle \hat{\xi}_s^2 \rangle = \int \frac{\hbar}{\rho\Omega} \coth\left(\frac{\hbar\Omega}{2k_B T}\right) D(\Omega) d\Omega. \quad (10)$$

where $D(\Omega) = 1/(2\pi)^2 \int d^2\mathbf{q} \delta(\Omega - \Omega_{\mathbf{q}})$ is the density of state of the sliding phonons. We regulate the divergence of the integral over Ω by a Debye frequency Ω_D cut-off chosen such that the degrees of freedom of the sliding motion per unit cell is conserved, i.e., $\int_{\Omega \leq \Omega_D} D(\Omega) d\Omega = 1/A_0$, which leads to

$$\Omega_D^2 = \Omega_0^2 + \frac{4\pi\sqrt{\mu(\lambda + 2\mu)}}{\rho A_0} \quad (11)$$

where A_0 is the unit-cell area. $\Omega_0 = \Omega_{\mathbf{q}=0}$ is the temperature- and field-dependent sliding phonon gap related to the polarization reversal (see below). Carrying out the integral in Eq. (10) leads to

$$\langle \hat{\xi}_s^2 \rangle = \frac{k_B T}{\pi\sqrt{\mu(\lambda + 2\mu)}} \ln \frac{\sinh \frac{\hbar\Omega_D}{2k_B T}}{\sinh \frac{\hbar\Omega_0}{2k_B T}} \equiv f(\langle \hat{u}_s \rangle, T). \quad (12)$$

A real Ω_0 demands that a physically stable phase of the system should fulfill the condition $3\langle \hat{u}_s \rangle^2 + 3f - a_0^2 > 0$. When $E = 0$, from Eq. (7) we have the paraelectric $\langle \hat{u}_s \rangle = 0$ and ferroelectric $\langle \hat{u}_s \rangle = \pm(a_0^2 - 3f)^{1/2}$ states for $3f > a_0^2$ and $3f \leq a_0^2$, respectively; When $E \neq 0$, always $\langle \hat{u}_s \rangle \neq 0$ (see Eq. (7)) and

$$\langle \hat{u}_s \rangle^2 = a_0^2 - 3f(\langle \hat{u}_s \rangle, T) + \frac{ZE a_0^4}{4\Delta \langle \hat{u}_s \rangle} \quad (13)$$

TABLE I. The parameter γ and Curie temperature T_c calculated for several sliding bilayer ferroelectrics with model parameters extracted from first-principles calculations [1, 3, 26, 27].

	Δ	λ	μ	A_0	ρ	a_0	P_0	γ	T_c
WTe ₂	1.37×10^{-2}	1.89	2.69	21.8	68.18	0.246	0.38	1.69	660
h-BN	1.67	3.37	7.67	5.38	7.81	0.72	2.08	0.71	1.58×10^4
Units	meV/Å ²	eV/Å ²	eV/Å ²	Å ²	10^{-7} kg/m ²	Å	pC/m	10^{-2}	K

which coincides with the ferroelectric case when $E = 0$ but $\langle \hat{u}_s \rangle \neq 0$. The gap of the sliding phonons under the different conditions are

$$\Omega_0 = \frac{2}{a_0^2} \sqrt{\frac{2\Delta}{\rho}} \begin{cases} (3f - a_0^2)^{1/2}, & E = 0, \langle \hat{u}_s \rangle = 0 \\ \left[2\langle \hat{u}_s \rangle^2 + \frac{Za_0^4 E}{4\Delta \langle \hat{u}_s \rangle} \right]^{1/2}, & \text{otherwise} \end{cases} \quad (14)$$

In the ferroelectric phase without the field (i.e., $E = 0$ and $\langle \hat{u}_s \rangle \neq 0$), Eq. (14) implies that Ω_0 softens with increasing temperature by the average amplitude $|\langle \hat{u}_s \rangle|$ but then increases with temperature in the paraelectric phase via $(3f - a_0^2)^{1/2}$, indicating a dip in $\Omega_0(T)$ at the Curie temperature (T_c). We shall show that this softening leads to an abnormal specific heat at T_c .

In the following, we solve Eq. (13) self-consistently together with Eq. (11) and Eq. (14). Its first term represents the spontaneous sliding in the absence of fluctuations that according to the second term is reduced by thermal and zero-point fluctuations. The last term in Eq. (13) is the Stark effect.

Spontaneous ferroelectricity. We investigate the spontaneous sliding ferroelectrics without an external field. At zero temperature, the ferroelectricity persists only when the zero-point fluctuations do not destroy the order, i.e., $\langle \hat{u}_s \rangle^2 = a_0^2 - 3f(\langle \hat{u}_s \rangle, T = 0) > 0$, which leads to the condition

$$\gamma \equiv \frac{\hbar}{(\rho A_0)^{1/2} [\mu(\lambda + 2\mu)]^{1/4} a_0^2} < \frac{\sqrt{\pi}}{3} \quad (15)$$

that does not require ferroelectricity and holds for any sliding structural phase transitions. The parameter γ measures the ratio of the mean-square amplitude of zero-point fluctuations to the squared distance between minimum energy states. $\gamma = \sqrt{\pi}/3$ marks a quantum phase transition and when $\gamma > \sqrt{\pi}/3$ a quantum paraelectric state occurs as in SrTiO₃ and KTaO₃ [28–30]. Eq. (15) states that bilayers with large unit-cell mass (ρA_0), high intralayer stiffness and a large distance between sliding minima favour the order. According to Table I, the zero-point fluctuations are not important for WTe₂ and h-BN bilayers, as expected. At any finite temperatures, $\Omega_0 \rightarrow 0$ and $f(\langle \hat{u}_s \rangle, T \neq 0) \rightarrow \infty$ when $\Delta \rightarrow 0$, which implies the absence of order as follows from the Mermin-Wagner theorem [19]. Here we predict a stricter condition for a sliding phase transition, *viz.* not only $\Delta > 0$ but also $\gamma < \sqrt{\pi}/3$.

We next address the thermal dynamics of robust sliding ferroelectrics such as WTe₂ and h-BN bilayers, in which $\gamma \ll \sqrt{\pi}/3$. At low temperatures $k_B T \ll \hbar \Omega_0$ and $E = 0$, the small fluctuations ($3f$) on the right-hand side of Eq. (13) may be approximated by $\langle \hat{u}_s \rangle \approx \pm a_0 [1 - 3f(a_0^2, T)/(2a_0^2)]$, which leads to

$$\langle \hat{u}_s(T) \rangle = \langle \hat{u}_s(0) \rangle - \frac{3k_B T}{2\pi \sqrt{\mu(\lambda + 2\mu)} a_0} \exp\left(-\frac{\hbar \Omega_0}{k_B T}\right) \quad (16)$$

where $\langle \hat{u}_s(0) \rangle \approx \pm a_0 [1 - 3\gamma/(2\sqrt{\pi})]$. In a ferroelectric ($Z \neq 0$) the associated pyroelectric coefficient reads

$$\frac{\partial \langle P(T) \rangle}{\partial T} = -\frac{3k_B Z}{2\pi \sqrt{\mu(\lambda + 2\mu)} a_0} \frac{\hbar \Omega_0}{k_B T} \exp\left(-\frac{\hbar \Omega_0}{k_B T}\right), \quad (17)$$

which differs from the $T^{-1/2}$ prefactor found for 3D ferroelectrics [25, 31]. Eq. (16) predicts reduced polarization at thermal energies far below the sliding phonon gap $\Omega_0 \approx (4/a_0)(\Delta/\rho)^{1/2}$.

Higher temperatures and larger fluctuations increasingly reduce the polarization. $\langle \hat{u}_s \rangle$ does not vanish until the infrared divergence of $\lim_{\langle \hat{u}_s \rangle \rightarrow 0} f(\langle \hat{u}_s \rangle, T \neq 0)$, i.e., the critical fluctuations signals the phase transition, which indicates a first-order sliding phase transition, see Fig. 2(a). We estimate the Curie temperature T_c by the condition $\lim_{T \rightarrow T_c^-} \partial \langle \hat{u}_s \rangle / \partial T \rightarrow \infty$. T_c solves Eq. (13) with $E = 0$

$$2\langle \hat{u}_s \rangle + 3 \frac{\partial f(\langle \hat{u}_s \rangle, T_c)}{\partial \langle \hat{u}_s \rangle} = 0 \quad (18)$$

$$\langle \hat{u}_s \rangle^2 - a_0^2 + 3f(\langle \hat{u}_s \rangle, T_c) = 0. \quad (19)$$

In h-BN and WTe₂ bilayers $\hbar \Omega_D \ll k_B T_c \ll \mu(\lambda + 2\mu)a_0^4/(A_0 \Delta)$ such that

$$T_c = \frac{2\pi T_0}{3(1 + \ln[1 + \pi^2 T_0^2 / (6T_c T_\Delta)])} \quad (20)$$

$$\langle \hat{u}_s \rangle |_{T=T_c^-} = \pm a_0 \sqrt{\frac{3T_c}{2\pi T_0}} \quad (21)$$

where $k_B T_0 = \sqrt{\mu(\lambda + 2\mu)} a_0^2$ is a measure of the energy cost of flipping an individual local dipole while $k_B T_\Delta = A_0 \Delta$ is the barrier per unit cell when switching the entire polarization coherently. The predicted first-order phase transition agrees with the conclusion for R-stacked WSe₂ bilayer [32].

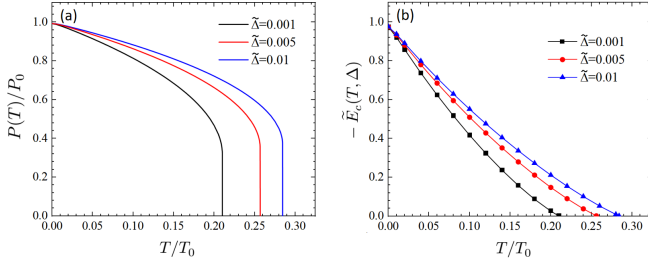


FIG. 2. (a) The polarization $P(T)$ and (b) the critical switching field $-\tilde{E}_c$ normalized by $8\Delta/(3\sqrt{3}P_0)$ as a function of temperature for various dimensionless switching barriers $\tilde{\Delta} = A_0\Delta/k_B T_0$, where we adopt $\gamma = 0.01$.

Intrinsic switching field. Shorted metallic gates such as graphene on both sides of the ferroelectric screen the ferroelectric dipoles, while a voltage bias generates the electric field E in Eq. (1). The screening modifies the electrostatic interactions and stabilizes a single domain configuration compared to the ungated situation, but otherwise does not affect the physics. According to Eq. (13) the (non-linear) ferroelectric susceptibility

$$\begin{aligned} \chi(T, E) &= Z \frac{\partial \langle \hat{u}_s(T, E) \rangle}{\partial E} \\ &= \frac{Z^2 a_0^4}{8\Delta \langle \hat{u}_s \rangle^2} \left[1 + \frac{3}{2\langle \hat{u}_s \rangle} \frac{\partial f}{\partial \langle \hat{u}_s \rangle} + \frac{Z a_0^4 E}{8\langle \hat{u}_s \rangle^3 \Delta} \right]^{-1}. \end{aligned} \quad (22)$$

A large external field against the polarization destabilizes the ferroelectric order by decreasing the phonon gap until it switches at a coercive field E_c determined by $\lim_{E \rightarrow E_c} \chi(T, E) \rightarrow \infty$:

$$E_c(T, \Delta) = -\frac{8\Delta \langle \hat{u}_s \rangle_c^3}{Z a_0^4} \left[1 + \frac{3}{2\langle \hat{u}_s \rangle_c} \frac{\partial f(\langle \hat{u}_s \rangle_c, T)}{\partial \langle \hat{u}_s \rangle_c} \right]. \quad (23)$$

where $\langle \hat{u}_s \rangle_c$ follows from Eq. (13) for $E = E_c$, i.e.,

$$3\langle \hat{u}_s \rangle_c^2 = a_0^2 - 3 \left[f(\langle \hat{u}_s \rangle_c, T) + \langle \hat{u}_s \rangle_c \frac{\partial f(\langle \hat{u}_s \rangle_c, T)}{\partial \langle \hat{u}_s \rangle_c} \right]. \quad (24)$$

Since $\partial f(\langle \hat{u}_s \rangle, T)/\partial \langle \hat{u}_s \rangle^2 < 0$

$$-E_c < \frac{8\Delta \langle \hat{u}_s \rangle_c^3}{Z a_0^4} \equiv -E_0 \quad (25)$$

where $\Omega_0(T, E_0) = 0$. The ferroelectric order therefore switches before the gap vanishes, in contrast to bulk ferroelectrics in which $\Omega_0(E_c) = 0$, i.e., at relatively low coercive fields in spite of the high thermal stability.

Figure 2(b) displays numerical solutions of Eq. (23) and Eq. (24) for $E_c(T, \Delta)$ as a function of temperature for various Δ with E_c normalized by the classical switching field $8\Delta/(3\sqrt{3}P_0)$ in the absence of any fluctuations.

$E_c(T, \Delta)$ is well fitted by the power law

$$E_c(T, \Delta) = -\frac{8\Delta}{3\sqrt{3}P_0} \left(1 - \frac{3\gamma}{\sqrt{\pi}} \right)^{3/2} \left(1 - \frac{T}{T_c} \right)^\eta \quad (26)$$

The first term in brackets on the r.h.s. represents the effect of quantum fluctuations. The second one is a Curie-Weiss Law with fitted critical exponent $\eta \approx 1.35$, which is slightly smaller than that of bulk ferroelectrics with a second-order phase transition ($\eta = 1.5$) [33]. E_c is real when the ferroelectric order is stable, i.e. when $\gamma < \sqrt{\pi}/3$ and $T < T_c$, as it should. The above coercive field holds for the coherent switching of a single ferroelectric domain [33, 34] and is of order $\sim 1 - 10$ GV/m for WTe₂ and h-BN bilayers. This number is an order of magnitude larger than observed switching fields [4, 6, 7]. Structural disorder such as dislocations and twisting should reduce the switching field, but their modelling is beyond the scope of the present paper.

Electrocaloric effect and specific heat. The electrocaloric effect refers to temperature changes caused by the adiabatic (de)polarization of the ferroelectric order by applied electric fields. The effect is especially large around first-order phase transitions and interesting for heat management applications [35]. The entropy of an ensemble of non-interacting bosons reads

$$S(T, E) = k_B \sum_{\mathbf{q}} [(1 + n_{\mathbf{q}}) \ln(1 + n_{\mathbf{q}}) - n_{\mathbf{q}} \ln n_{\mathbf{q}}] \quad (27)$$

where $n_{\mathbf{q}} = \{\exp[\hbar\Omega_{\mathbf{q}}/(k_B T)] - 1\}^{-1}$ is the Planck distribution of the sliding phonons. The isothermal field derivative of entropy then reads

$$\frac{\partial S(T, E)}{\partial E} = -\frac{\rho A k_B}{4\pi \sqrt{(\lambda + 2\mu)\mu}} \frac{\partial \Omega_0^2}{\partial E} \int_{x_0}^{x_D} \frac{x e^x}{(e^x - 1)^2} dx \quad (28)$$

where A is the area of bilayer and $x_{0(D)} = \hbar\Omega_{0(D)}/(k_B T)$. Figure 3 shows the entropy change $\Delta s(E)$ (per unit mass) as a function of the external electric field at $T = T_c^+$ for WTe₂ and h-BN bilayers, where $\lim_{E \rightarrow 0^+} T_c \Delta s(E)$ corresponds to the latent heat freed by the polarization of the dipoles. $\Delta s(E)$ is significant for the h-BN bilayer being of the order of $\text{JK}^{-1}\text{kg}^{-1}$, but two orders of magnitude smaller in the WTe₂ bilayer.

For temperature-independent Lamé parameters, the specific heat of the sliding phonons at a fixed electric field reads

$$\begin{aligned} C_E = T \frac{\partial S}{\partial T} &= \frac{\rho A k_B^3 T^2}{2\pi \hbar^2 \sqrt{(\lambda + 2\mu)\mu}} \int_{x_0}^{x_D} \frac{x^3 e^x}{(e^x - 1)^2} dx \\ &\quad - \frac{\rho A k_B T}{4\pi \sqrt{(\lambda + 2\mu)\mu}} \frac{\partial \Omega_0^2}{\partial T} \int_{x_0}^{x_D} \frac{x e^x}{(e^x - 1)^2} dx. \end{aligned} \quad (29)$$

The first term in Eq. (29) follows from the conventional 2D Debye model, while the second one reflects the softening of Ω_0 and is singular at the phase transition since

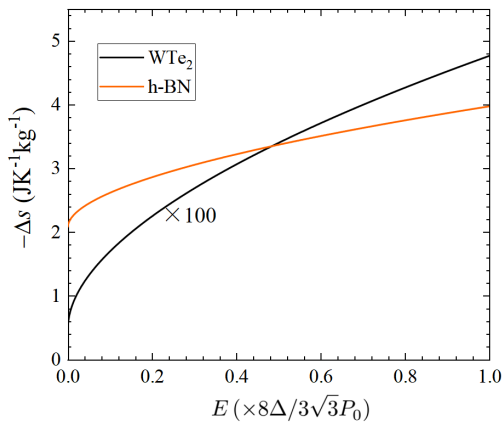


FIG. 3. The entropy change per unit mass $\Delta s(E)$ with the electric field at $T = T_c^+$, where the field is in unit of $8\Delta/(3\sqrt{3}P_0)$. $\lim_{E \rightarrow 0^+} T_c \Delta s(E)$ corresponds to the latent heat generated by the polarization of disordered dipoles.

$\partial\Omega_0^2/\partial T|_{T=T_c^-} \propto \partial(\dot{u}_s)^2/\partial T|_{T=T_c^-} \rightarrow \infty$. This divergent specific heat might be observed in the associated anomalous heat transport that is beyond the scope of our paper.

Discussion. We can compare the sliding ferroelectricity with 2D magnetism. In contrast to usual magnets, the zero-point fluctuations explicitly reduces the sliding ferroelectric order and Curie temperature, because in magnetic systems quantum spins rather than classical magnetic dipoles order and a nonvanishing magnon gap is already a sufficient condition for an phase transition [36]. Otherwise, at low temperatures Eq. (16) resembles the magnetization of 2D ferromagnets as limited by magnon excitations [37]. Here the polarization decreases with temperature due to “ferrons”, i.e. phonon excitations that carry electric dipoles [31, 38, 39]. We find an explicit expression for the reduction of the classical ground state polarization Za_0 by zero-point as well as thermal fluctuations. At sufficiently low temperatures $\langle P(T) \rangle \simeq Za_0[1 - 3/(2a_0^2)f(a_0^2, T)]$, hence the electric dipole carried by a single sliding phonon with wave vector \mathbf{q} is $\delta p_{\mathbf{q}} = -3\hbar Z/(\rho a_0 \Omega_{\mathbf{q}})$. We can rewrite Eq. (16) as $\langle P(T) \rangle = \langle P(0) \rangle - \int d^2\mathbf{q}/(2\pi)^2 \delta p_{\mathbf{q}} n_{\mathbf{q}}$.

Eq. (20) is similar to that of the 2D magnets after replacing the exchange interaction by $\sqrt{\mu(\lambda + 2\mu)}a_0^2$ or $k_B T_0$ [40, 41]. We now understand the stability of sliding ferroelectricity in terms of the high intralayer stiffness that governs the energy scale needed to destroy its order $k_B T_0$ ($\sim 0.1 - 1$ eV), which is much larger than the 2D magnetic exchange interaction ($\lesssim 10$ meV). The estimates of the critical temperatures in Table I $T_c = 660$ K ($T_c = 1.58 \times 10^4$ K) for WTe₂ (h-BN) bilayers agree qualitatively with experiments that report $T_c \sim 350$ K for WTe₂ [4] and a nearly temperature-

independent polarization of the BN bilayer in a wide temperature range up to room temperature [6].

The present minimal model of sliding phase transitions can be extended and improved by numerical modelling. Here we consider only unidirectional lateral sliding, which is analogous to a one-component polarization approximation in the Landau-Ginzburg-Devonshire theory [42]. We may refine this model by including the coupling with other degrees of freedom, e.g., flexural and transverse in-plane displacements. The continuum mechanics is not accurate when the temperatures exceed the Debye temperature and should be checked by lattice dynamical calculations. Disorder can give rise to position-dependent switching fields and stick-slip domain formation. The structural stability of twisted states that generate Moiré patterns in van der Waals bilayers can be addressed by an appropriate generalization for transitions that involve small twist angles [43–45].

Conclusion: We model the thermodynamics of 2D sliding ferroelectrics driven by an external field in a continuum mean-field approximation. We explain the high Curie temperatures of recently discovered ferroelectrics in spite of ultralow switching fields. We predict a critical specific heat and a scaling law between the cohesive electric field and temperature. The combination of ultralow switching field and high T_c endows the 2D sliding ferroelectrics with unique functionality for potential applications in high-integration nanoelectronics.

Acknowledges: P. T. and G. B. are supported by JSPS KAKENHI Grant No. 19H00645 and G. B. is also supported by 22H04965.

-
- [1] L. Li and M. Wu, Binary compound bilayer and multilayer with vertical polarizations: Two-dimensional ferroelectrics, multiferroics, and nanogenerators, *ACS Nano* **11**, 6382 (2017).
 - [2] Q. Yang, M. Wu, and J. Li, Origin of two-dimensional vertical ferroelectricity in WTe₂ bilayer and multilayer, *J. Phys. Chem. Lett.* **9**, 7160 (2018).
 - [3] X. Liu, Y. Yang, T. Hu, G. Zhao, C. Chen, and W. Ren, Vertical ferroelectric switching by in-plane sliding of two-dimensional bilayer WTe₂, *Nanoscale* **2019** 11, 18575 (2019).
 - [4] Z. Fei, W. Zhao, T. A. Palomaki, B. Sun, M. K. Miller, Z. Zhao, J. Yan, X. Xu, and D. H. Cobden, Ferroelectric switching of a two-dimensional metal, *Nature* **560**, 336 (2018).
 - [5] P. Sharma, F. Xiang, D. Shao, D. Zhang, E. Y. Tsybal, A. R. Hamilton, J. Seidel, A room-temperature ferroelectric semimetal, *Sci. Adv.* **5**, eaax5080 (2019).
 - [6] K. Yasuda, X. Wang, K. Watanabe, T. Taniguchi, and P. Jarillo-Herrero, Stacking-engineered ferroelectricity in bilayer boron nitride, *Science* **372**, 1458 (2021).
 - [7] M. V. Stern, Y. Waschitz, W. Cao, I. Nevo, K. Watanabe, T. Taniguchi, E. Sela, M. Urbakh, O. Hod, M. B. Shalom, Interfacial ferroelectricity by van der Waals slid-

- ing, *Science* **372**, 1462 (2021).
- [8] M. Wu and Ju Li, Sliding ferroelectricity in 2D van der Waals materials: Related physics and future opportunities, *Proceedings of the National Academy of Sciences* **118**, e2115703118 (2021).
- [9] X. Wang, K. Yasuda, Y. Zhang, S. Liu, K. Watanabe, T. Taniguchi, J. Hone, L. Fu, and Pablo Jarillo-Herrero, Interfacial ferroelectricity in rhombohedral-stacked bilayer transition metal dichalcogenides, *Nature Nanotechnology* **17**, 367 (2022).
- [10] J.-U. Lee, S. Lee, J. H. Ryoo, S. Kang, T. Y. Kim, P. Kim, C.-H. Park, J.-G. Park, and H. Cheong, Ising-Type Magnetic Ordering in Atomically Thin FePS, *Nano Lett.* **16**, 7433 (2016).
- [11] B. Huang, G. Clark, E. Navarro-Moratalla, D. R. Klein, R. Cheng, K. L. Seyler, D. Zhong, E. Schmidgall, M. A. McGuire, D. H. Cobden, W. Yao, D. Xiao, P. Jarillo-Herrero, and X. Xu, Layer-dependent ferromagnetism in a van der Waals crystal down to the monolayer limit, *Nature (London)* **546**, 270 (2017).
- [12] C. Gong, L. Li, Z. Li, H. Ji, A. Stern, Y. Xia, T. Cao, W. Bao, C. Wang, Y. Wang, Z. Q. Qiu, R. J. Cava, S. G. Louie, J. Xia, and X. Zhang, Discovery of intrinsic ferromagnetism in two-dimensional van der Waals crystals, *Nature (London)* **546**, 265 (2017).
- [13] Z. Fei, B. Huang, P. Malinowski, W. Wang, T. Song, J. Sanchez, W. Yao, D. Xiao, X. Zhu, A. F. May, W. Wu, D. H. Cobden, J. H. Chu, and X. Xu, Z. Fei, B. Huang, P. Malinowski, W. Wang, T. Song, J. Sanchez, Two-dimensional itinerant ferromagnetism in atomically thin Fe_3GeTe_2 *Nat. Mater.* **17**, 778 (2018).
- [14] M. Bonilla, S. Kolekar, Y. Ma, H. C. Diaz, V. Kalappattil, R. Das, T. Eggers, H. R. Gutierrez, M.-H. Phan, and M. Batzill, Strong room-temperature ferromagnetism in VSe2 monolayers on van der Waals substrates *Nat. Nanotechnol.* **13**, 289 (2018).
- [15] D. J. O'Hara, T. Zhu, A. H. Trout, A. S. Ahmed, Y. K. Luo, C. H. Lee, M. R. Brenner, S. Rajan, J. A. Gupta, D. W. McComb, and R. K. Kawakami, Room Temperature Intrinsic Ferromagnetism in Epitaxial Manganese Selenide Films in the Monolayer Limit, *Nano Lett.* **18**, 3125 (2018).
- [16] Y. Deng, Y. Yu, Y. Song, J. Zhang, N. Z. Wang, Z. Sun, Y. Yi, Y. Z. Wu, S. Wu, J. Zhu, J. Wang, X. H. Chen, and Y. Zhang, Gate-tunable room-temperature ferromagnetism in two-dimensional Fe_3GeTe_2 , *Nature* **563**, 94 (2018).
- [17] C. Huang, J. Feng, F. Wu, D. Ahmed, B. Huang, H. Xiang, K. Deng, and E. Kan, Toward Intrinsic Room-Temperature Ferromagnetism in Two-Dimensional Semiconductors, *Journal of the American Chemical Society* **140**, 11519 (2018).
- [18] W. Li, X. Qian, and J. Li, Phase transitions in 2D materials, *Nat. Rev. Mater.* **6**, 829 (2021).
- [19] N. D. Mermin and H. Wagner, Absence of ferromagnetism or antiferromagnetism in one- or two-Dimensional isotropic Heisenberg models, *Phys. Rev. Lett.* **17**, 1133 (1966).
- [20] P. C. Hohenberg, Existence of long-range order in one and two dimensions. *Phys. Rev.* **158**, 383 (1967).
- [21] H. Suzuura and T. Ando, Phonons and electron-phonon scattering in carbon nanotubes, *Phys. Rev. B* **65**, 235412 (2002).
- [22] P. L. de Andres, F. Guinea, and M. I. Katsnelson, Bending modes, anharmonic effects, and thermal expansion coefficient in single-layer and multilayer graphene, *Phys. Rev. B* **86**, 144103 (2012).
- [23] R. Ribeiro-Palau, C. Zhang, K. Watanabe, T. Taniguchi, J. Hone, and C. Dean, Twistable electronics with dynamically rotatable heterostructures, *Science* **361**, 690 (2018).
- [24] M. E. Lines, Correlated-effective-field theory: A statistical approach for grossly anharmonic lattice vibrations, *Phys. Rev. B* **9**, 950 (1974).
- [25] A. M. Glass and M. E. Lines, Low-temperature behavior of spontaneous polarization in LiNbO_3 and LiTaO_3 , *Phys. Rev. B* **13**, 180 (1976).
- [26] B. Sachs, T. O. Wehling, M. I. Katsnelson, and A. I. Lichtenstein, Adhesion and electronic structure of graphene on hexagonal boron nitride substrates, *Phys. Rev. B* **84**, 195414 (2011).
- [27] E. Torun, H. Sahin, S. Cahangirov, A. Rubio, and F. M. Peeters, Anisotropic electronic, mechanical, and optical properties of monolayer WTe_2 , *J. Appl. Phys.* **119**, 074307 (2016).
- [28] K. A. Müller and H. Burkard, SrTiO_3 : An intrinsic quantum paraelectric below 4 K, *Phys. Rev. B* **19**, 3593 (1979).
- [29] S. E. Rowley, L. J. Spalek, R. P. Smith, M. P. M. Dean, M. Itoh, J. F. Scott, G. G. Lonzarich, and S. S. Saxena, Ferroelectric quantum criticality, *Nature Phys* **10**, 367 (2014).
- [30] Tobias Esswein and Nicola A. Spaldin, Ferroelectric, quantum paraelectric or paraelectric? Calculating the evolution from BaTiO_3 to SrTiO_3 to KTaO_3 using a single-particle quantum-mechanical description of the ion, [arXiv:2112.11284](https://arxiv.org/abs/2112.11284) (2021).
- [31] P. Tang, R. Iguchi, K. Uchida, G.E.W. Bauer, Excitations of the ferroelectric order, [arXiv:2203.06367](https://arxiv.org/abs/2203.06367) (2022).
- [32] Y. Liu Song Liu, Baichang Li, Won Jong Yoo, and James Hone, Identifying the Transition Order in an Artificial Ferroelectric van der Waals Heterostructure, *Nano Lett.* **22**, 1265 (2022).
- [33] S. Ducharme, V. M. Fridkin, A. V. Bune, S. P. Palto, L. M. Blinov, N. N. Petukhova, and S. G. Yudin, Intrinsic Ferroelectric Coercive Field, *Phys. Rev. Lett.* **84**, 175 (2000).
- [34] V. M. Fridkin and S. Ducharme, General features of the intrinsic ferroelectric coercive field, *Physics of the Solid State* **43**, 1320 (2001).
- [35] Y. Liu James F. Scott, and Brahim Dkhil, Direct and indirect measurements on electrocaloric effect: Recent developments and perspectives, *Appl. Phys. Rev.* **3**, 031102 (2016).
- [36] We consider here the thermodynamic limit of infinitely extended systems, which should be distinguished from the field and temperature dependent dynamics of large but finite magnetic particles that give rise to the phenomenon of superparamagnetism, see e.g. <https://en.wikipedia.org/wiki/Superparamagnetism>
- [37] P. Bruno, Spin-wave theory of two-dimensional ferromagnets in the presence of dipolar interactions and magnetocrystalline anisotropy *Phys. Rev. B* **43**, 6015 (1991).
- [38] G. E. W. Bauer, R. Iguchi, and K. Uchida, Theory of transport in ferroelectric capacitors, *Phys. Rev. Lett.* **126**, 187603 (2021).
- [39] P. Tang, R. Iguchi, K. Uchida, G.E.W. Bauer, Thermo-

- electric Polarization Transport in Ferroelectric Ballistic Point Contacts, *Phys. Rev. Lett.* **128**, 047601 (2022).
- [40] J. L. Lado and J. Fernández-Rossier, On the origin of magnetic anisotropy in two dimensional CrI_3 , *2D Mater.* **4**, 035002 (2017).
- [41] M. Bander and D. L. Mills, Ferromagnetism of ultrathin films, *Phys. Rev. B* **38**, 12015(R) (1988).
- [42] P. Chandra and P. B. Littlewood, A Landau Primer for Ferroelectrics, *Physics of Ferroelectrics* **105**, 69 (2007).
- [43] F. Peymanirad, S. Singh, H. Ghorbanfekr-Kalashami, K. Novoselov, F. Peeters, and M. Neek-Amal, Thermal activated rotation of graphene flake on graphene, *2D Mater.* **4**, 025015 (2017).
- [44] S. Bagchi, H. T. Johnson, and H. B. Chew, Rotational stability of twisted bilayer graphene, *Phys. Rev. B* **101**, 054109 (2020).
- [45] S. Zhu, E. Annevelink, P. Pochet, and H. T. Johnson, Selection rules of twistrionic angles in two-dimensional material flakes via dislocation theory, *Phys. Rev. B* **103**, 115427 (2021).